Guidelines for nano-scale stray magnetic field measurements

Authors

Hans W. Schumacher, Sibylle Sievers, Gaoliang Dai, Xiukun Hu, Manuela Gerken

Physikalisch-Technische Bundesanstalt, Bundesallee 100, 38116 Braunschweig, Germany

Olga Kazakova, Robb Puttock, Hector Corte, Craig Barton

National Physical Laboratory, Teddington TW110LW, United Kingdom

Petr Klapetek, Marek Havlíček, Miroslav Valtr, Michal Ulvr

Czech Metrology Institute, Brno 638 00, Czech Republic

Volker Neu

Leibniz-Institut für Festkörper- und Werkstoffforschung Dresden, Helmholtzstraße 20, 01069 Dresden, Germany

Baha Sakar

Department of Physics, Gebze Technical University, Gebze, 41400, Kocaeli, Turkey

Scope of guide

The object of this guide is to define and describe the general principles and the details of the reference materials for traceable high resolution magnetic stray field measurements and the calibration procedures. This includes description and technical details of the reference materials that can be used for MFM method calibration. Calibration procedures and detailed uncertainty evaluation are also described.

Contents

Introduction

Today, local magnetic stray field measurements with resolution from above 50 µm down to below 500 nm can be realized by scanning magnetic field (SMF) methods including scanning Hall magnetometry, scanning MR magnetometry etc. and magneto optical indicator film (MOIF) microscopy. However, currently calibration schemes of these two methods rely on determining the sensor response to a homogeneous magnetic field, which doesn't allow for high spatial calibrations. To obtain reliable calibrations with high spatial resolution the influence of the response of the non-punctiform sensor in strongly spatially varying fields has to be considered and needs to be implemented into the calibration procedures.

Magnetic force microscopy (MFM) can be considered as the standard tool for nano scale investigations of the local magnetic properties of magnetic nanostructures, thin films and devices. However, despite of its wide use MFM measurements per se only deliver purely qualitative stray field images that cannot be applied for quantitative data analysis. Furthermore, the measured signal strongly depends on properties of the magnetic tip making even reliable qualitative analysis a complex task. Hence a calibration that includes the characterization of the magnetic tip is needed.

This guideline aims to provide industry end users, instrument manufactures and Calibration Laboratories the description of traceable calibration procedures based on reference materials with well defined local stray field distribution for all three methods. The guideline includes sample information, key parameters which need to be collected, artifacts which possibly occur during the MFM measurements due to the interaction between a magnetic tip and a sample, and a detailed process to tell users how to perform MFM measurements.

Magnetic stray field reference materials

Magnetic probes for high resolution microscopic analysis are non punctiform i.e. they have a finite spatial extension. When the typical dimensions of magnetic structures are of the same order of magnitude as the extension of the probe the measured signal is determined by a convolution of the probe properties with the spatially varying stray field distribution. Hence, calibrations in homogeneous fields do not provide sufficient information for traceable high resolution measurements. While spatially resolved stray field measurements tools (e.g. MOIF systems) are nowadays calibrated in homogeneous fields a qualitative test of their spatial resolution is often performed by imaging the stray field of magnetic encoders. Encoders consist of magnetic materials with up and down magnetized regions that generate a spatially varying stray field with periodicity down to 100 µm. However such encoders can show significant variations of the stray field distribution from device to device inhibiting their use as quantitative reference materials. Here, a novel stray field reference materials based on lithographically patterned hard magnetic materials will be described. The lithographic definition will allow high reproducibility, full dimensional traceability, calculable stray field properties and increased pattern resolution down to 10 µm.

Typical MFM calibration materials do not cover a sufficient span of the feature size from several µm to the nm range required for overlapping validation of traceability from high resolution MFM measurements to µm resolved techniques such as MOIF or scanning Hall

microscopy. Here, reference materials with variable magnetic pattern size from about 1 µm down to below 10 nm will be described. By means of calibrations measurement performed on these extended length scales, allows evaluating the traceability of stray field measurements from measurement techniques with overlapping resolution.

Reference materials for MFM measurement

Reference sample for tip calibration

The reference sample used for magnetic tip calibration should have stable magnetic properties, exhibit very well defined perpendicular magnetic anisotropy. Furthermore, the reference sample should also exhibit different spatial frequency components of the domain size, such that the calibration of the reference sample includes information of the spatial frequencies of interest as those present in the unknown sample to be measured.

One of the good candidate calibration samples for MFM measurement is Co/Pt multilayer sample (d4015_0916) which has been used as a calibration sample in one round robin comparison of quantitative MFM measurement as its domain or stray field pattern can be quantitatively constructed from the measured MFM data without detailed knowledge of the yet to be calibrated probe. In the presented here, the multilayers are prepared by magnetron sputtering with the following layer architecture Pt(2nm)/[(Co(0.4nm)/Pt(0.9nm)]$_{100}$/Pt(5nm)/Ta(5nm)/SiOx/Si(100). The total thickness of the magnetic layer is 130 nm and owing to the interface anisotropy of the thin Co layers the film develops magnetic anisotropy perpendicular to the surface. In zero applied magnetic field the magnetization of the multilayer collapses into a band domain pattern with average domain width of 170 nm. Global magnetization measurements determine the saturation magnetization to be M_s=500 kA/m (error +- 30 kA/m) and confirm the perpendicular magnetization through a ratio $Q_u = K_u/K_d \geq 2.5$ (K_u = 0.4 MJ/m^3 is the perpendicular anisotropy constant, $K_d = ½\ \mu_0 M_s^2$ = 0.16 MJ/m^3 is the magnetostatic energy density). The Bloch type domain transition has a width of about 16 nm. The band domain pattern of the reference sample develops homogeneously across the whole sample surface, thus in case of the tip calibration measurement specifying the measurement region is not necessary.

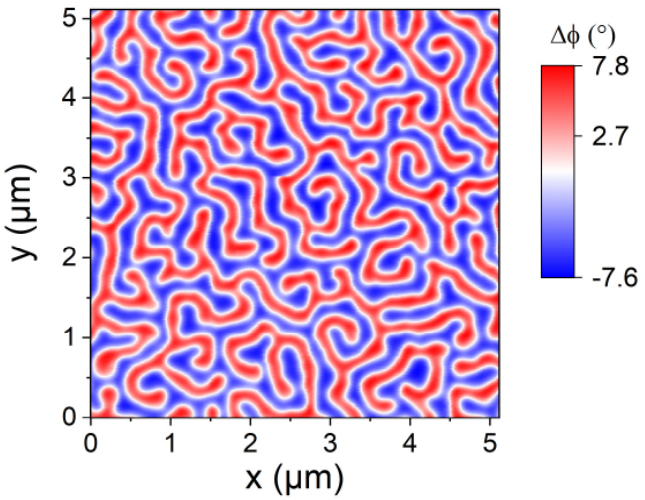

Fig. 1 Example of the MFM image of the reference sample d4015_0916 used in the NanoMag project for tip calibration.

Reference sample for stray field measurement

SmCo721 sample and patterned d5099 sample should be used as a reference samples for stray field measurement.

The sample d5099 is a Co/Pt multilayer sample prepared by magnetron sputtering. The layer architecture is Pt(2nm)/[(Co(0.53nm)/Pt(1.32nm)]$_{10}$/Pt(5nm) Ta(15nm)/SiOx /Si(100) and the total thickness of the magnetic layer is 18.6 nm. The saturation moment per unit area is determined to m_s/area = 1.04×10^{-4} A (error +- 0.1×10^{-4} A), corresponding to a saturation magnetization of M_s=560 kA/m (error +- 55 kA/m) with the given thickness. Due to the interface anisotropy at the Co/Pt interfaces the multilayer develops a perpendicular magnetic anisotropy with magnetization direction within individual domains normal to the sample surface.

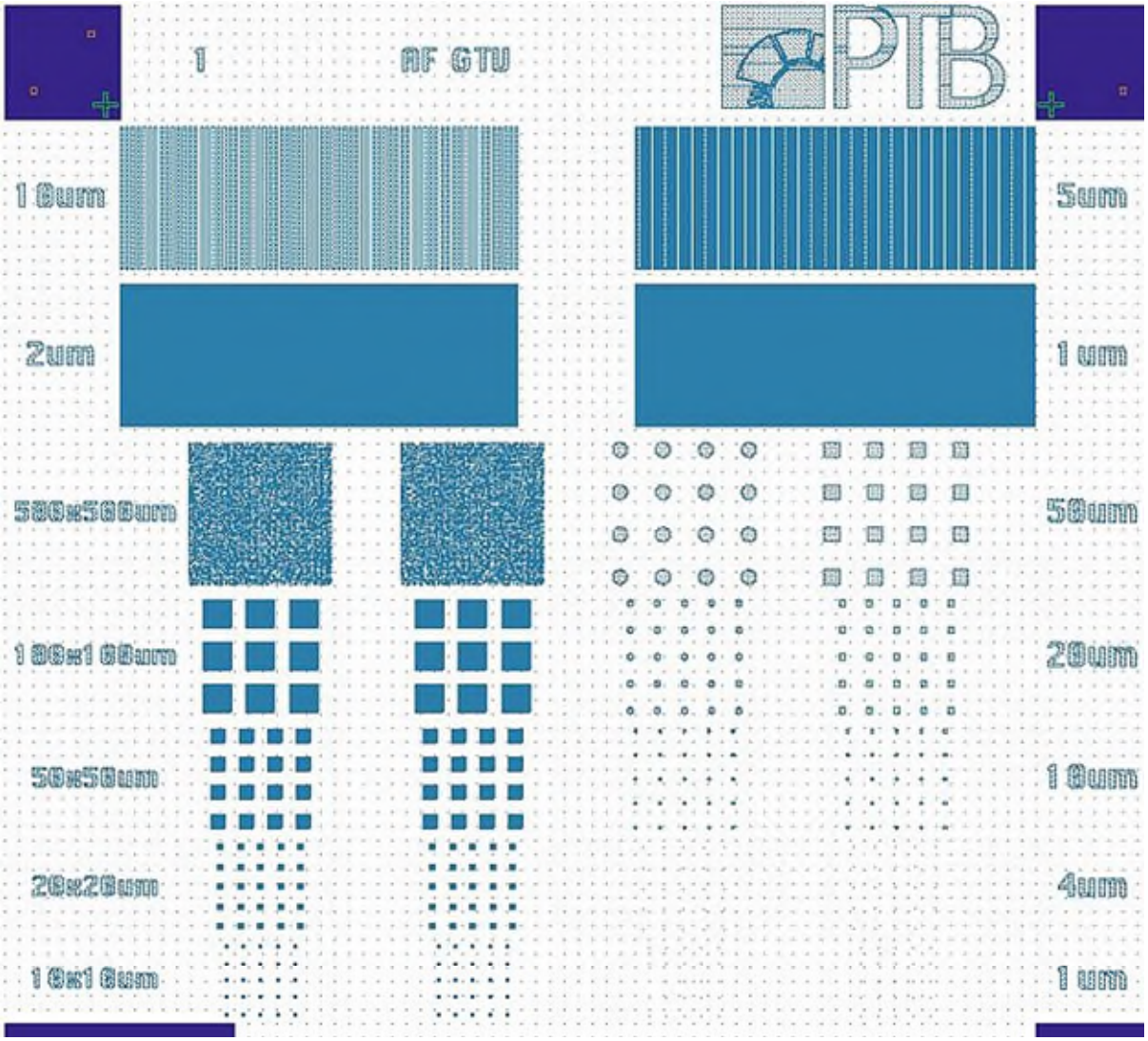

Fig. 2 Layout of the lithography mask with various patterns (disks, bars, squares, maze patterns) of different length scales.

The SmCo721 sample is an epitaxially grown film of the hexagonal $SmCo_5$ phase, with c-axis orientation normal to the film plane. The film was prepared by UHV pulsed laser deposition (PLD) on a heated (650°C), Ru-buffered Al_2O_3 substrate. The full layer architecture is Ta(3nm)/SmCo5(12nm)/Ru(9nm)/Al2O3(0001) and the epitaxial relation is <11-20>(0001)$SmCo_5$||<11-20>(0001)Ru||<10-10>(0001)Al_2O_3 [1]. Due to the large uniaxial magnetocrystalline anisotropy of the $SmCo_5$ phase with easy magnetization direction along the c-axis, the film develops strong perpendicular magnetic anisotropy. In the as-prepared state, the sample shows patchy domains with individual domains normal to the sample surface.

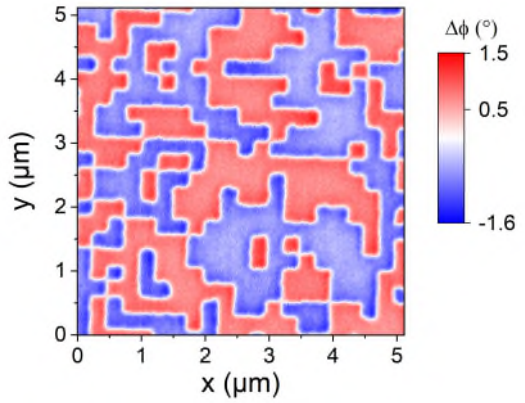

Fig. 3 Example of the MFM image of the reference sample d5099 after patterning.

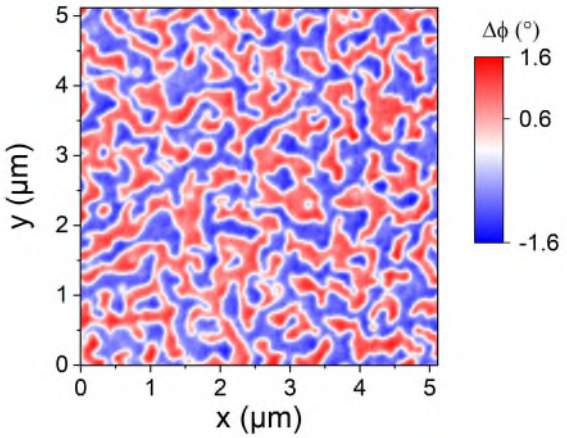

Fig. 4 Example of the MFM image of the reference sample SmCo721 in the as-prepared state.

Calibration procedures/measurement of magnetic stray field

MFM

To quantitatively evaluate stray fields above a magnetic sample surface by using magnetic force microscope (MFM), magnetic tip must firstly be calibrated on a reference sample [2-8]. Magnetic tip was calibrated by using a Co/Pt multilayered film as a reference sample which shows stable well-known magnetic properties and well-defined perpendicular band domains.

The tip transfer function (d*Hz*/dz of the tip at tip apex) was obtained by performing a regularized deconvolution process in the Fourier domain with a Wiener filter [9] and the L-curve method [10] for determining a suitable regularization parameter to get a physically reasonable result. The calibrated tip was then applied for MFM imaging on a test sample. After applying similar deconvolution process, a traceable quantitative determination of the stray fields of the test sample were obtained.

Key parameters

Besides the information of the reference sample, some key parameters for later data analysis need to be collected and defined before MFM measurements.

a) Spring constant of the cantilever

This parameter can be obtained i) from the description of the tip provider, e.g. Nanosensors (PPP-MFMR) which gives this value for each tip; ii) theoretically from the calculation based on the cantilever geometry [11]; iii) from thermal noise method, e.g., in the JPK SPM software; iv) from metrological calibration of the spring constant of AFM cantilever [12].

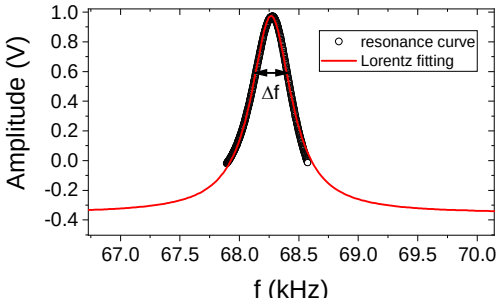

Fig. 5 Resonance curve of a cantilever.

b) Quality factor Q of the tip

This parameter can be obtained from the resonance curve of the tip as shown in Fig. 5. From this curve Q is calculated as $= f_0/\Delta f$, where f_0 is the resonance frequency, Δf is the full bandwidth at 0.707 of the maximum amplitude [13].

The value should be estimated for each MFM measurement.

c) Sensitivity of the setup

Since the deflection of the cantilever is displayed in Volts, to know the oscillation amplitude of the tip in nm in the tapping mode, a force curve between a cantilever tip and a bare hard substrate is used to determine the sensitivity of the setup. The force curve is normally performed on a hard material with clean surface, negligible magnetic or electrostatic interactions with the probe, e.g., on a silicon substrate. A typical curve (taken from Nanoscope IIIa) is shown in Fig. 6. From the linear fitting of the curve (blue line), the sensitivity of the cantilever can be calculated in nm/V. This value can be used to convert the deflection data into nanometers, also can be used to set the oscillation amplitude as actual nanometers of oscillation.

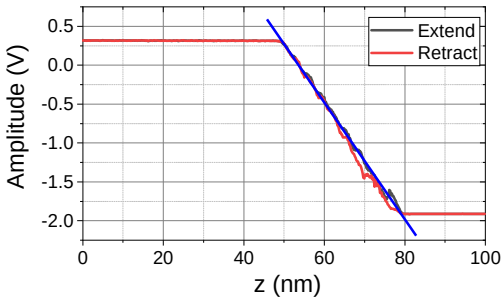

Fig. 6 Force plot of a cantilever. Fitting the linear transition region to get the sensitivity of the setup.

The drive amplitude is chosen to result in an oscillation amplitude during the MFM scan of about 20 – 40 nm.

d) Tip-Sample distance

The sensitivity of the setup is used to determine the tip-sample distance in MFM measurements. One needs to calculate the oscillation amplitude A_0 when the tip approaches on the surface. The tip-sample distance will be equal to A_0 + lift height (setup gives).

For the tip calibration, closer the tip approaches to the sample surface, more information of the tip could be obtained. Considering the cleanness of the sample surface and oscillation amplitude of the tip, the tip-sample distance is typically set to be ~60 nm.

e) Scan size

For the tip calibration on the reference, considering the domain size of the reference sample and the size of tip radius, the measured area for tip calibration was taken as 5.11 µm × 5.11 µm with 512 × 512 pixels (i.e. a pixel size of ~ 10 nm).

f) Canting angle of the cantilever in the setup

The canting angle of the cantilever needs to be obtained for the used MFM setup, e.g., from the manufacturer. Generally, it will be about 10°, e.g., for Nanoscope IIIa.

g) Magnetization orientation of the tip

The best way to magnetize the tip is before MFM measurements. On one hand, it ensures correct representation of the stray field vector direction of the sample in the MFM image. On the other hand, this information could be used to avoid disarranging domain structure of the test sample due to the strong stray field of some type of magnetic tips.

Artefacts in MFM measurements

Since MFM employs the interaction between magnetic tip and magnetic sample, some artifacts resulting from the magnetic interaction are inevitable. They must be ruled out to ensure that a tip calibration process can be successfully performed. Some typical artifacts are illustrated in the following.

a) MFM on the sample with strong stray field

When the coercivity field of the tip is low, e.g. ~30 mT for Nanosensors PPP-MFMR, and the stray field of the sample is strong, the magnetization of the tip could be switched. Typical images are shown in Fig. 7.

In Fig. 7(a), many “blue points” (e.g., as indicated by the black arrow in Fig. 7(a)) in the red stripes can be observed. It indicates that the magnetization orientation of the tip is opposite to that of the sample in the red regions. When the tip locates at these positions, the

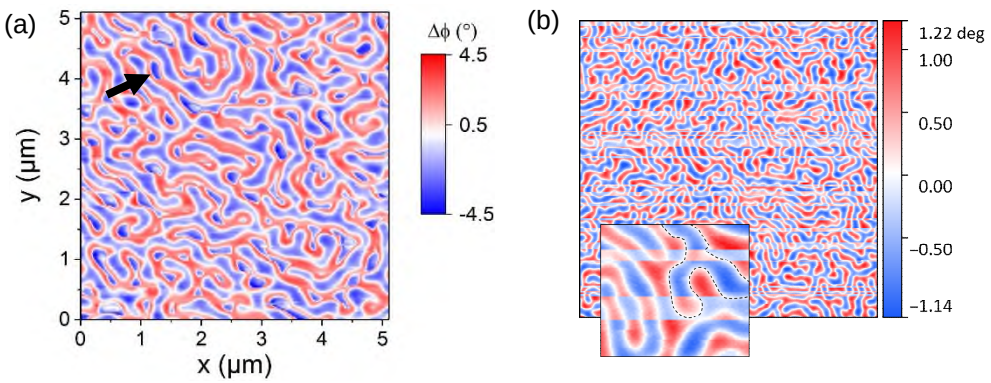

Fig. 7 Typical MFM images when the tip is switched by the strong stray field of the sample.

magnetization of the tip near the tip apex is switched. When the tip moves to the blue regions, the reversed part of the tip switches back.

Another type of the influence can be seen in Fig. 7(b). A few lines seem to be shifted corresponding to the "true" domain structure.

b) MFM on the sample with low coercivity

When the stray field of the tip is strong and the coercivity of the sample is low, the tip can switch the magnetization of the sample. Figure 8 shows two MFM images (a) and (b) taken from consecutive MFM measurements. The original domain structure was a large single domain with the magnetization orientation in the opposite direction of that of the tip (with the red color), as indicated by the lower part in Fig. 8(a). However, during the MFM measurements, the single domain structure was gradually disarranged by the strong stray field of the tip into a multidomain structure. In this case, the magnetization orientation of the tip

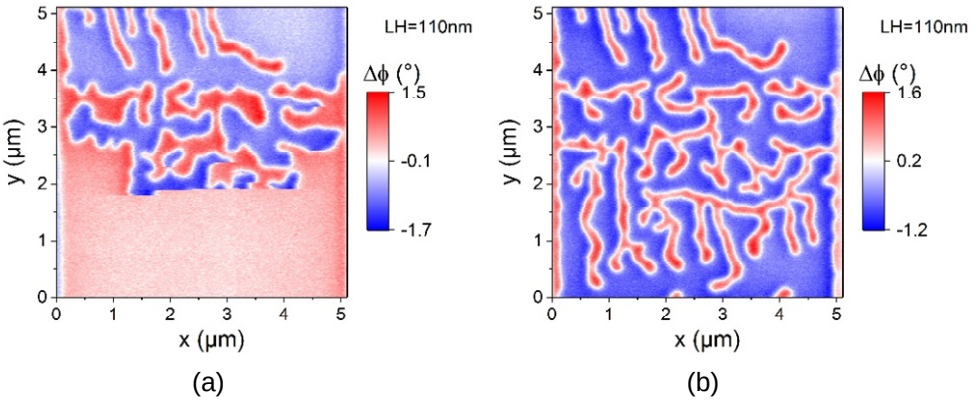

Fig. 8 Typical MFM images when domain of the sample is switched by the strong stray field of the tip.

should be set in the same direction of the single domain to ensure the original domain structure can be evaluated.

c) Distortion of domain structure

Figure 9 shows a typical distortion of domain structure of the reference sample. The domain structure shows obviously wrong features. One type of domain is much broader than the other. Such image could not be used for the tip calibration.

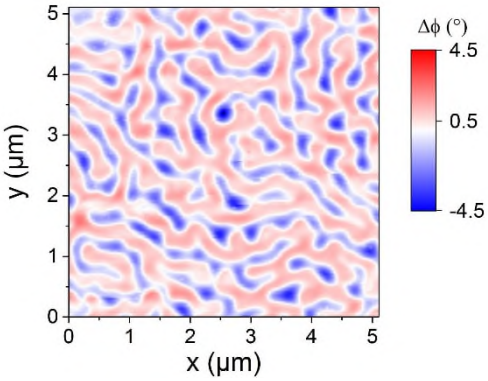

Fig. 9 Typical distortion of MFM image.

In summary, there may be more artefacts occurring in MFM measurements, depending on the magnetic properties of the test sample. Distinguishing the correct domain structure from the MFM image representation structure relies on how well the user know the magnetic properties of the test sample. To get rid of the influence of artifacts is the precondition of the tip calibration and stray field evaluation processes.

Quantitative MFM measurements and Analysis

The quantification of stray fields by qMFM (quantitative MFM) require a tip calibration and the stray field evaluation of the sample under study. The tasks can be separated in measurement procedures and analysis procedures.

a)Tip calibration

The magnetic tip is calibrated by using the reference sample. The tip transfer function (dHz/dz of the tip at a certain distance from the tip apex) is obtained by performing a regularized deconvolution process in the Fourier domain. The detailed algorithm is shown in the **Appendix A**. Take an MFM image (data: phase in °) of the reference sample at a defined tip-sample distance and with a defined scan size. Evaluate the tip transfer function according to Software Guideline (Gwyddion, self-programmed codes, or other programs).

b) Stray field evaluation of the test sample

The calibrated tip was then applied to MFM imaging on the test sample. After applying similar deconvolution process, a traceable quantitative determination of the stray fields of the test sample were obtained. The detailed algorithm is shown in the **Appendix A**.

Take an MFM image with the same parameters for the tip calibration (tip-sample distance, scan size and pixel number). Evaluate stray fields of the test sample according to Software Guideline (Gwyddion, self-programmed codes, or other programs).

The scan rate is recomended in the range of 2-10 µm/s.

Below is given the procedure applied for quantitative MFM in the course of this project. It is separated into measurement procedures and analysis procedures. For a recent overview see [14].

Measurement procedure

(Mi) Adjustment of probe's oscillation amplitude and resonance frequency
(Mii) Measure probe's resonance quality Q and spring constant C_{tip}
(Miii) (repeated) measurement of calibration sample with well-adjusted tip-sample distance. The Co/Pt multilayer sample introduced in chapter *Reference sample for tip calibration* was measured on a 5.11 µm x 5.11µm area with 512 x 512 pixel and with a tip-sample distance of 60 nm.
(Miv) Measurement of reference samples (patterned $[Co/Pt]_{10}$ and epitaxial SmCo5 film) with identical parameters
(Mv) (repeated) measurement of calibration sample with identical parameters.

Analysis procedure

The quantitative data analysis is performed either in SigMath [7], [8], Matlab [15] or Gwyddion [6]. In all cases, 2-dimensional data matrices obtained from measurements on flat surfaces are transformed in Fourier space, and appropriate operations are applied. Results are transformed back into real space. Simpler pre- and post- treatment of scanning probe data is performed with the scanning probe data analysis packages, e.g. WSxM [16] or Gwyddion [17]. The mathematical correlation between sample properties, probe properties and measured MFM data in Fourier space is given further below together with the uncertainty evaluation.

(Ai) Background (tilt/bow) correction of calibration data obtained in (Miii)

(Aii) Optional: correction of cantilever canting angle in the calibration data (see Appendix A 3.1)

(Aiii) Construction of stray field or surface charge pattern from corrected calibration measurements (see Appendix A 3.2)

(Aiv) Deconvolution: the tip transfer function (2-dimensional d*Hz*/dz *profile* of the probe at a chosable position below the tip apex) was obtained by performing a regularized deconvolution process in the Fourier domain with a Wiener filter [9] and the L-curve method [10] for determining a suitable regularization parameter to get a physically reasonable result (see Appendix A 3.1).

(Av) Repeat (Ai) to (Aiv) for all calibration measurements
Only when the TTFs from (Miii) and (Mv) agree to within a tolerable margin, the averaged TTF can be taken as a representative of the tip's imaging property during step (Miv)

(Avi) Optional: smooth RSTTF either by circular averaging or segmental averaging along concentric rings around the TTF maximum.

(Avii) Background correction of MFM data from reference sample obtained in M(iv)

(Aviii) Deconvolution of corrected MFM data with agreed TTF from step (Av). This results in the desired quantitative surface charge or stray field pattern of the sample. Note: the effect of lever canting angle (theta), resonance quality (Q) and cantilever spring constant (C_{tip}) cancel in the deconvolution process, when above values can be considered constant throughout the measurement sequence (uninterrupted measurement).

(Aix) Alternative: develop a hypothetical surface charge/stray field model of the sample and construct a theoretical MFM pattern via convolution with above TTF. Modify model until sufficient agreement is achieved.

Uncertainty evaluation [18], [19]

Uncertainty evaluation of TTF

TTF for the uncertainty evaluation is taken as d*Hz*/dz of the tip at tip apex. The uncertainty evaluation of TTF consists of type A and type B components. Type A uncertainty is obtained by 13 independent measurements on the reference sample. Type B evaluation concerns following input quantities and their standard deviation: phase signal of the MFM image $\Delta\Phi$, pixel size δA, tip quality factor Q, tip spring constant C_{tip}, saturation magnetization of the reference sample M_s, thickness of the reference sample h, tip-sample distance z, and regularization parameter α. The detailed information can be seen in the **Appendix B**.

Uncertainty evaluation of the stray field

Type B evaluation of the stray field concerns following input quantities and their standard deviations: phase signal of the MFM image $\Delta\Phi$ and $u_{\Delta\Phi}$, pixel size δA and $u_{\delta A}$, tip quality factor Q and u_Q, tip spring constant Ctip and u_{Ctip}, calibrated tip *TTF* and u_{TTF}, and regularization parameter α and u_α. The detailed information can be seen in the **Appendix B**.

APPENDIX A: Algorithm

1. Involved mathematical knowledge

$$f(z) = \int g(x)h(x+z)dx$$

$$F(\omega) = \int\int g(x)h(x+z)dx\, e^{-i\omega z}dz = \int\int g(x)h(y)e^{-i\omega(y-x)}dy\,dx$$

$$= \int h(y)e^{-i\omega y}dy \int g(x)e^{i\omega x}\,dx = H(\omega)G(-\omega) = H(\omega)\hat{G}(\omega)$$

where the hat ^ refers to the complex conjugate.

Continuous FFT to discrete FFT:

$$F(u,v) = \iint f(x,y)e^{-iux-ivy}dxdy = \sum_{m=0}^{M-1}\sum_{n=0}^{N-1} f(m,n)e^{-2\pi(i\frac{u}{M}m+j\frac{v}{N}n)}\,\Delta x\Delta y$$

$$= \delta A_{pixel}F(u,v)_{DFFT}$$

where the additional term δA_{pixel} is the pixel area.

Modified Bessel function of the first Kind:

$$I_1(x) = \frac{x}{2}\left(1 + \frac{1}{2!}\left(\frac{x}{2}\right)^2 + \frac{1}{3!\,2!}\left(\frac{x}{2}\right)^4 + \frac{1}{4!\,3!}\left(\frac{x}{2}\right)^6 + \frac{1}{5!\,4!}\left(\frac{x}{2}\right)^8 + \cdots\right)$$

2. Interaction between tip and sample

2.1 considering M_{sample}, $\partial H_{\text{tip}}/\partial z$ (default in the range of NanoMag project)

$$E(r,z) = -\mu_0 \int_{tip} M_{sample}(r+r',z)H_{tip}(r',z)dr'dz'$$

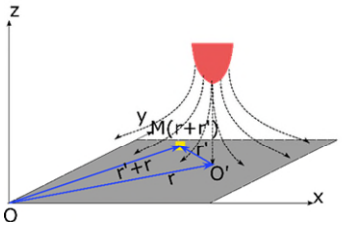

$$F_z(r,z) = -\frac{\partial E(r,z)}{\partial z}$$

$$= \mu_0 \int M_{sample}(r+r',z)\frac{\partial H_{tip}(r',z)}{\partial z}dr'dz'$$

$$\frac{\partial F_z}{\partial z}(r,z) = \mu_0 \int_{tip} M_{sample}(r+r',z)\frac{\partial H_{tip}(r',z)}{\partial z}dr'$$

$$\frac{\partial F_z}{\partial z}(k,z) = \mu_0 \frac{\partial \hat{H}_{tip}}{\partial z}(k,z)M_{sample}(k,z)$$

In DFFT,

$$\frac{\partial F_z}{\partial z}(k,z) = \mu_0\delta A_{pixel} \times M_{sample}(k,z)$$

$$\times \frac{\partial \hat{H}_{tip}}{\partial z}(k,z)$$

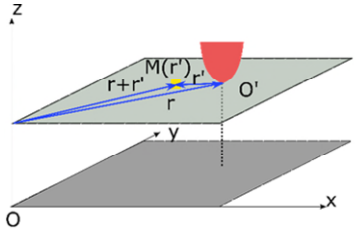

2.2 Considering M_{tip}, $\partial H_{sample}/\partial z$ (optional)

The magneto static energy of the whole system:

$$E(r,z) = -\mu_0 \int M_{tip}(r',z) H_{sample}(r+r',z) dr'\, dz'$$

The force acting on the tip is

$$F_z(r,z) = -\frac{\partial E(r,z)}{\partial z} = \mu_0 \int M_{tip}(r',z) \frac{\partial H_{sample}(r+r',z)}{\partial z} dr' dz'$$

$$\frac{\partial F_z}{\partial z}(r,z) = \mu_0 \int M_{tip}(r',z) \frac{\partial H_{sample}(r+r',z)}{\partial z} dr'$$

$$\frac{\partial F_z}{\partial z}(k,z) = \mu_0 \widehat{M}_{tip}(k,z) \frac{\partial H_{sample}}{\partial z}(k,z)$$

In the Fourier space,

$$\frac{\partial F_z}{\partial z}(k,z)\Big|_{DFFT} = \mu_0 \delta A_{pixel} \times \widehat{M}_{tip}(k,z)\Big|_{DFFT} \times \frac{\partial H_{sample}}{\partial z}(k,z)\Big|_{DFFT}$$

3. Tip transfer function based on 2.1

3.1 Phase signal

MFM signal in unit degree can be written as:

$$\Delta\phi(r,z) = -\frac{180}{\pi} \cdot \frac{Q}{C_{tip}} \cdot \frac{\partial F_z}{\partial z}(r,z)$$

Note that, if the minus sign should be used or not depends on the MFM setup. User needs to check it. For example, when the magnetization orientations of the tip and the sample align in the same direction, the force is attractive. The force gradient $\partial F_z/\partial z(r,z)$ is positive with regard to the tip. If the setup give a minus phase shift, the minus sign must exist.

In DFFT,

$$\Delta\phi(k,z) = -\mu_0 \cdot \frac{180}{\pi} \cdot \frac{Q \cdot \delta A_{pixel}}{C_{tip}} M_{sample}(k,z) \times \frac{\partial \widehat{H}_{tip}}{\partial z}(k,z)$$

For a thin film consisting of a single layer,

$$M_{sample}(k,z) = M_S m(k) \cdot (1 - e^{-kh}) \cdot e^{-kz}$$

here, M_S and h are the saturation magnetization and the thickness of the sample, m is normalized thickness-independent magnetization distribution, respectively.

The stray field gradient generated by the sample at z can be written as:

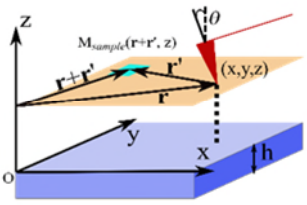

$$H_S^z(k,z) = \frac{(1-e^{-kh})e^{-kz}}{2} M_S m(k)$$

$$\frac{\partial H_S^z}{\partial z}(k,z) = -k\frac{(1-e^{-kh})e^{-kz}}{2} M_S m(k)$$

Considering the cantilever canting angle correction:

$$LCF(k,\theta) = \begin{Bmatrix} \frac{-ik_y sin\theta}{k} - cos\theta & cantilever\ axis\ in\ the\ y\ direction \\ \frac{-ik_x sin\theta}{k} - cos\theta & cantilever\ axis\ in\ the\ x\ direction \end{Bmatrix}$$

(For example, the direction from cantilever head to the bottom in + *x* direction as shown in figure, θ > 0, otherwise θ>0.)

Considering the driving amplitude A_0 of the tip, define ã=A_0 k LCF*(k,θ)*, the cantilever canting angle correction factor becomes [20]:

$$[LCF]^2 = [LCF(k,\theta)]^2\left[1 + \frac{1}{2!}\left(\frac{\tilde{a}}{2}\right)^2 + \frac{1}{3!\,2!}\left(\frac{\tilde{a}}{2}\right)^4 + \frac{1}{4!\,3!}\left(\frac{\tilde{a}}{2}\right)^6 + \frac{1}{5!\,4!}\left(\frac{\tilde{a}}{2}\right)^8 \ldots\right]$$

$$k_x = 2\pi \times \frac{u - \frac{M}{2}}{M\delta x};\ k_y = 2\pi \times \frac{v - \frac{N}{2}}{N\delta y};\quad k = \sqrt{k_x^2 + k_y^2}$$

$$\Delta\emptyset(k,z) = -\mu_0 \cdot \frac{180}{\pi} \cdot \frac{Q \cdot \delta A_{pixel}}{C_{tip}} M_S [LCF]^2 m(k,0) \cdot (1-e^{-kh}) \cdot e^{-kz}\frac{\partial \hat{H}_{tip}}{\partial z}(k,z)$$

From the Fourier transform, k is averaged circularly. From the highest point of k-Amplitude curve we can get the periodicity of the stripe domain (up and down domains together), then the width of one stripe can be calculated.

$$w_D = \frac{\lambda}{2} = \frac{\pi}{k}$$

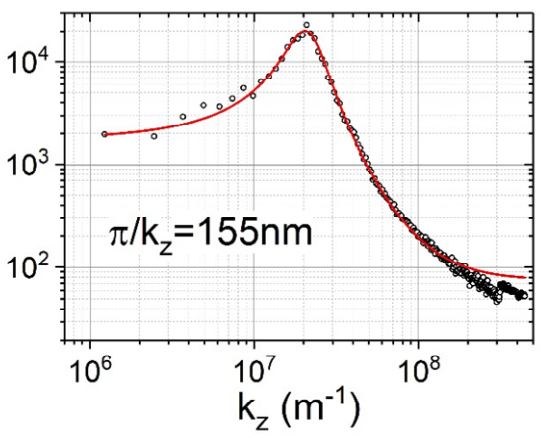

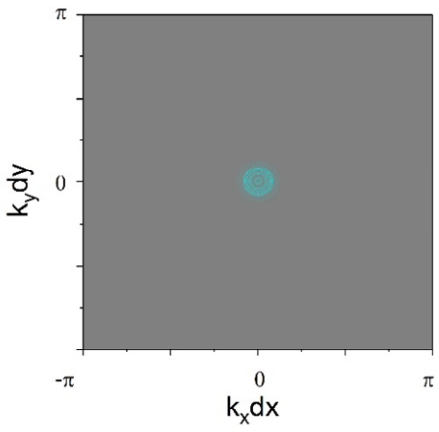

3.2 Magnetic charge distribution

This effective magnetic charge can be obtained after the discrimination from the experimental MFM image.

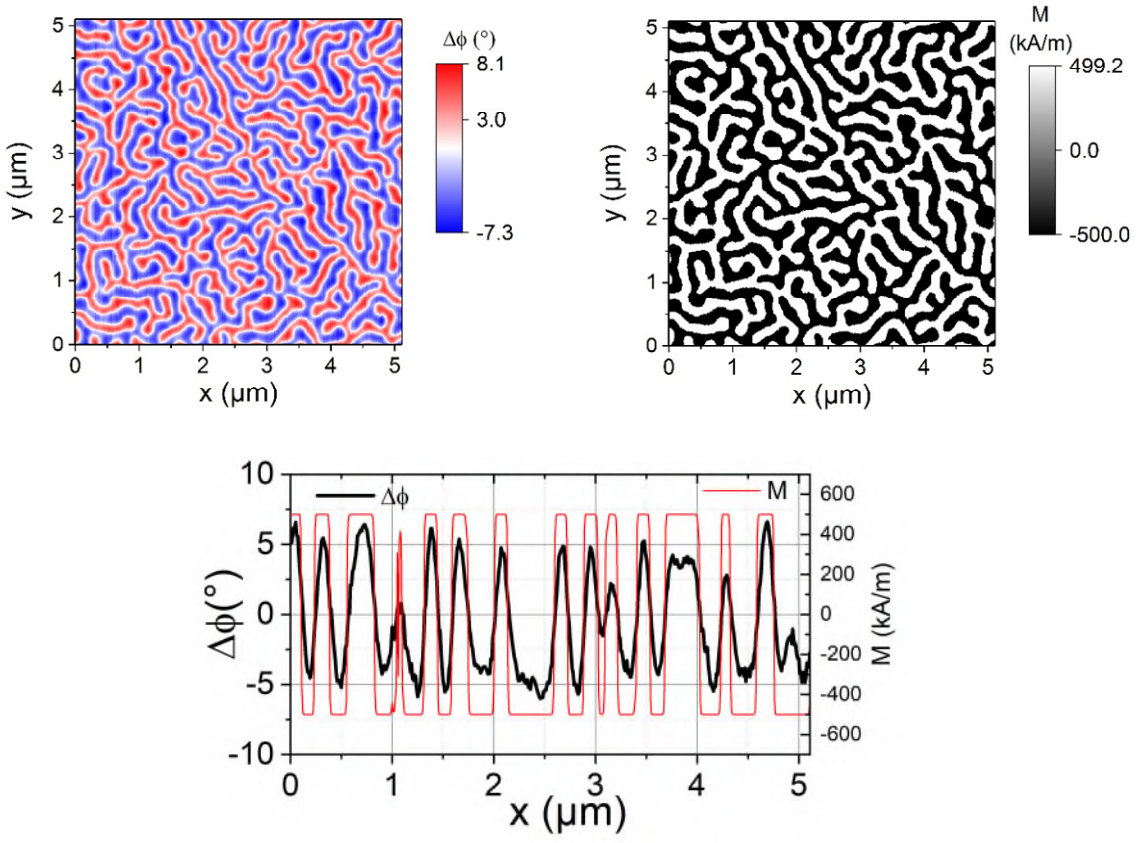

In the domain wall (DW) region, the z-component of magnetization [21] is:

$$m_z(r) = \tanh\left(\frac{\pi r}{\delta_{DW}}\right)$$

The following function is convoluted with M_{dis} can give this smooth transition of the magnetization:

$$f(x,y) = \operatorname{sech}^2\left(\frac{\pi\sqrt{x^2+y^2}}{\delta_{DW}}\right) = \operatorname{sech}^2\left(\frac{\pi r}{\delta_{DW}}\right)$$

$$\int \operatorname{sech}^2 cx\, dx = \frac{1}{c}\tanh(cx)$$

$$m_z(r) = \frac{\int_{-\frac{\delta_{DW}}{2}}^{\frac{\delta_{DW}}{2}} \operatorname{sech}^2\left(\frac{\pi r}{\delta_{DW}}\right) m_{dis}(r)dr}{\int_{-\infty}^{\infty} \operatorname{sech}\left(\frac{\pi r}{\delta_{DW}}\right) m_{dis}(r)dr} = \frac{\int_{-r}^{r} \operatorname{sech}^2\left(\frac{\pi r}{\delta_{DW}}\right) dr}{\frac{\delta_{DW}}{\pi}} = \tanh\left(\frac{\pi r}{\delta_{DW}}\right)$$

The equivalent normalized magnetization distribution at certain distance above the sample surface z can be calculated as:

$$m_{eff}(k,z) = \frac{(1-e^{-kh})e^{-kz}}{2} m(k)$$

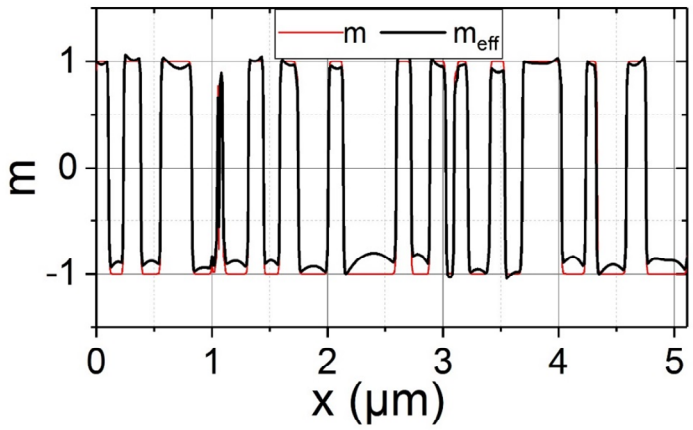

3.3 Wiener filter for deconvolution process [9]

Define:

$$C_0 = \mu_0 \cdot \frac{180}{\pi} \cdot \frac{Q \cdot \delta A_{pixel}}{C_{tip}} M_S$$

$$\Delta\phi(\boldsymbol{k},z) = -C_0[LCF(\boldsymbol{k},\theta)]^2 m(\boldsymbol{k})(1-e^{-kh})e^{-kz}\frac{\widehat{\partial H}_{tip}(\boldsymbol{k},z)}{\partial z}.$$

$$G(\boldsymbol{k},z) \equiv \Delta\phi(\boldsymbol{k},z),$$

$$H(\boldsymbol{k},z) \equiv -[LCF(\boldsymbol{k},\theta)]^2 m(\boldsymbol{k})(1-e^{-kh})e^{-kz},$$

$$F(\boldsymbol{k},z) \equiv C_0\frac{\widehat{\partial H}_{tip}(\boldsymbol{k},z)}{\partial z},$$

$$TTF(\boldsymbol{k},z) = \frac{1}{C_0}\hat{F}(\boldsymbol{k},z)$$

Corresponding to the Wiener deconvolution formula:

$$G(\boldsymbol{k},z) = H(\boldsymbol{k},z)F(\boldsymbol{k},z)$$

$$F(\boldsymbol{k},z) = \boldsymbol{G}(\boldsymbol{k},z)\frac{\hat{H}(\boldsymbol{k},z)}{|H(\boldsymbol{k},z)|^2+\alpha}$$

Here, α is constant.

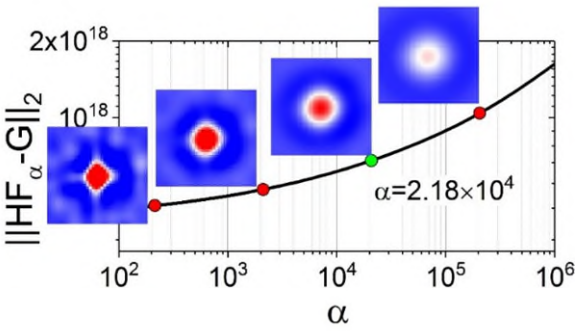

As shown in the figures, with decreasing α the difference between experimental and restored data tends to zero. It indicates that the Wiener deconvolution process prefers to give a zero noise to let the restored image $\boldsymbol{F_\alpha H}$ match with the input MFM image $\boldsymbol{G}$. However, with decreasing α the tip loses the reasonable profile.

In the deconvolution process, the α value is chosen via the L-curve criterion [10]. Calculate the curvature of the L-curve, at the maximum point, we obtain the value of α.

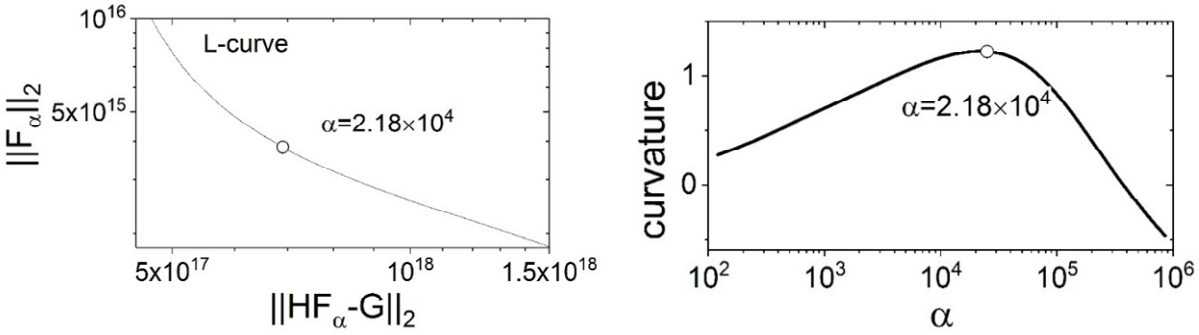

4. Stray field evaluation based on the calibrated tip
Define:

$$C_1 = \mu_0 \cdot \frac{360}{\pi} \cdot \frac{Q \cdot \delta A_{pixel}}{C_{tip}}$$

$$\Delta\phi(\boldsymbol{k}, z) = -C_1[LCF(\boldsymbol{k}, \theta)]^2 \left[\frac{\partial \widehat{H}_{tip}(\boldsymbol{k}, z)}{\partial z}\right] H_S^z(\boldsymbol{k}, z)$$

$$G(\boldsymbol{k}, z) \equiv \Delta\phi(\boldsymbol{k}, z),$$

$$H(\boldsymbol{k}, z) \equiv -[LCF(\boldsymbol{k}, \theta)]^2 \frac{\widehat{\partial H}_{tip}(\boldsymbol{k}, z)}{\partial z},$$

$$F(\boldsymbol{k}, z) \equiv C_1 H_z^S(\boldsymbol{k}, z),$$

$$H_z^S(\boldsymbol{k}, z) = \frac{1}{C_1} F(\boldsymbol{k}, z).$$

Repeat the process in 3.3, the stray fields of the test sample can be evaluated.

APPENDIX B: Uncertainty evaluation

1. Definition for the tip calibration
Relation between input quantities and measurands in the Fourier domain for the tip calibration:

$$\Delta\phi(\boldsymbol{k}, z) = -\mu_0 \cdot \frac{180}{\pi} \cdot \frac{Q \cdot \delta A_{pixel}}{C_{tip}} M_S [LCF(\boldsymbol{k}, \theta)]^2 m(\boldsymbol{k})(1 - e^{-kh}) e^{-kz} \frac{\widehat{\partial H}_{tip}(\boldsymbol{k}, z)}{\partial z}$$

Define:

$$C_0 = \mu_0 \cdot \frac{180}{\pi} \cdot \frac{Q \cdot \delta A_{pixel}}{C_{tip}} M_S$$

$$G(\boldsymbol{k},z) \equiv \Delta\phi(\boldsymbol{k},z),$$

$$H(\boldsymbol{k},z) \equiv -[LCF(\boldsymbol{k},\theta)]^2 m(\boldsymbol{k})(1-e^{-kh})e^{-kz},$$

$$F(\boldsymbol{k},z) \equiv C_0 \frac{\widehat{\partial H_{tip}(\boldsymbol{k},z)}}{\partial z},$$

$$TTF(\boldsymbol{k},z) = \frac{1}{C_0}\hat{F}(\boldsymbol{k},z)$$

Corresponding to the Wiener deconvolution formula:

$$G(\boldsymbol{k},z) = H(\boldsymbol{k},z)F(\boldsymbol{k},z)$$

$$F(\boldsymbol{k},z) = \boldsymbol{G}(\boldsymbol{k},z)\frac{\widehat{H}(\boldsymbol{k},z)}{|H(\boldsymbol{k},z)|^2+\alpha}$$

2. Definition for the stray field evaluation

Relation between input quantities and measurands in the Fourier domain for the tip calibration:

$$\Delta\phi(\boldsymbol{k},z) = -\mu_0 \cdot \frac{360}{\pi} \cdot \frac{Q\cdot\delta A_{pixel}}{C_{tip}}[LCF(\boldsymbol{k},\theta)]^2\left[\frac{\partial\widehat{H}_{tip}(\boldsymbol{k},z)}{\partial z}\right]H_S^z(\boldsymbol{k},z)$$

Define:

$$C_1 = \mu_0 \cdot \frac{360}{\pi} \cdot \frac{Q\cdot\delta A_{pixel}}{C_{tip}}$$

$$G(\boldsymbol{k},z) \equiv \Delta\phi(\boldsymbol{k},z),$$

$$H(\boldsymbol{k},z) \equiv -[LCF(\boldsymbol{k},\theta)]^2 \frac{\widehat{\partial H_{tip}(\boldsymbol{k},z)}}{\partial z},$$

$$F(\boldsymbol{k},z) \equiv C_1 H_z^S(\boldsymbol{k},z),$$

$$H_z^S(\boldsymbol{k},z) = \frac{1}{C_1}F(\boldsymbol{k},z)$$

Corresponding to the Wiener deconvolution formula:

$$G(\boldsymbol{k},z) = H(\boldsymbol{k},z)F(\boldsymbol{k},z)$$

$$F(\boldsymbol{k},z) = \boldsymbol{G}(\boldsymbol{k},z)\frac{\widehat{H}(\boldsymbol{k},z)}{|H(\boldsymbol{k},z)|^2+\alpha}$$

3. A type uncertainty evaluation

For the tip calibration: take *N* independent MFM images at different areas. Each image goes through the TTF calibration process to obtain TTF_i. The *TTF* average and the standard deviation of the mean *TTF* would be:

$$\overline{\boldsymbol{TTF}} = \frac{\boldsymbol{1}}{\boldsymbol{N}}\sum_{\boldsymbol{i=1}}^{\boldsymbol{N}} \boldsymbol{TTF_i}$$

$$\boldsymbol{u^2_{TTF\_A}} = \frac{\boldsymbol{1}}{\boldsymbol{N(N-1)}}\sum_{\boldsymbol{i=1}}^{\boldsymbol{N}} (\boldsymbol{TTF_i} - \overline{\boldsymbol{TTF}})^{\boldsymbol{2}}$$

For stray field evaluation: take *N* independent MFM images at different areas. Each image goes through the stray field determination process to obtain $H_Z^S{}_i$. The H_Z^S average $\overline{\boldsymbol{HZ}}$ and the standard deviation of the mean *HZ* would be:

$$\overline{\boldsymbol{HZ}} = \frac{\boldsymbol{1}}{\boldsymbol{N}}\sum_{\boldsymbol{i=1}}^{\boldsymbol{N}} \boldsymbol{HZ_i}$$

$$\boldsymbol{u^2_{HZ\_A}} = \frac{\boldsymbol{1}}{\boldsymbol{N(N-1)}}\sum_{\boldsymbol{i=1}}^{\boldsymbol{N}} (\boldsymbol{HZ_i} - \overline{\boldsymbol{HZ}})^{\boldsymbol{2}}$$

4. B type uncertainty evaluation

B type uncertainty evaluation concerns the propagation of uncertainty components between the real and Fourier domains and the Wiener filter applied in the deconvolution process in the Fourier domain.

4.1 Propagation of uncertainty from the real to the Fourier domain

The DFT for the real space data:

$$\chi_{kl} = \sum_{m=0}^{M-1}\sum_{n=0}^{N-1} X_{mn} e^{-i2\pi\frac{km}{M} - i2\pi\frac{ln}{N}}, \qquad k,l = 0,\dots,M-1,N-1$$

The real part:

$$R_{\chi_{kl}} = \sum_{m=0}^{M-1}\sum_{n=0}^{N-1} X_{mn}\cos\left(2\pi\frac{km}{M} + 2\pi\frac{ln}{N}\right), \qquad k,l = 0,\dots,M-1,N-1$$

The imaginary part:

$$S_{\chi_{kl}} = -\sum_{m=0}^{M-1}\sum_{n=0}^{N-1} X_{mn}\sin\left(2\pi\frac{km}{M} + 2\pi\frac{ln}{N}\right), \qquad k,l = 0,\dots,M-1,N-1$$

For each point in the Fourier space, sensitivity coefficients of input quantities X_{mn}:

The real part:

$$\frac{\partial R_{\chi_{kl}}}{\partial X_{mn}} = \cos\left(2\pi\frac{km}{M} + 2\pi\frac{ln}{N}\right)$$

The imaginary part:

$$\frac{\partial S_{\chi_{kl}}}{\partial X_{mn}} = -\sin\left(2\pi\frac{km}{M} + 2\pi\frac{ln}{N}\right)$$

Uncertainty of χ_{kl}:

The real part:

$$\boldsymbol{R}(\boldsymbol{u}^2_{\boldsymbol{\chi_{kl}}}) \equiv \sum_{m=0}^{M-1}\sum_{n=0}^{N-1}\left(\frac{\partial R_{\chi_{kl}}}{\partial X_{mn}}\right)^2 \boldsymbol{u}^2_{X_{mn}}$$

The imaginary part:

$$\boldsymbol{S}(\boldsymbol{u}^2_{\boldsymbol{\chi_{kl}}}) \equiv \sum_{m=0}^{M-1}\sum_{n=0}^{N-1}\left(\frac{\partial S_{\chi_{kl}}}{\partial X_{mn}}\right)^2 \boldsymbol{u}^2_{X_{mn}}$$

Uncertainties of $\boldsymbol{G}$ in the Fourier domain can be represented by the real and imaginary parts:

$$\boldsymbol{u}^2_{\boldsymbol{RG}} = \sum_{m=0}^{M-1}\sum_{n=0}^{N-1}\cos^2\left(2\pi\frac{km}{M} + 2\pi\frac{ln}{N}\right)\boldsymbol{u}^2_{G_{mn}}$$

$$\boldsymbol{u}^2_{\boldsymbol{SG}} = \sum_{m=0}^{M-1}\sum_{n=0}^{N-1}\sin^2\left(2\pi\frac{km}{M} + 2\pi\frac{ln}{N}\right)\boldsymbol{u}^2_{G_{mn}}$$

4.2 Propagation of uncertainty from the Fourier to the real domain

The inverse DFT for the real space data:

$$X_{mn} = \frac{1}{MN}\sum_{k=0}^{M-1}\sum_{l=0}^{N-1}\chi_{kl}e^{i2\pi\frac{km}{M}+i2\pi\frac{ln}{N}}, \qquad m,n = 0,\dots,M-1,N-1$$

Using the real and imaginary parts of χ_{kl}:

$$X_{mn} = \frac{1}{MN}\sum_{k=0}^{M-1}\sum_{l=0}^{N-1}\left[R_{\chi_{kl}}\cos\left(2\pi\frac{km}{M} + 2\pi\frac{ln}{N}\right) - S_{\chi_{kl}}\sin\left(2\pi\frac{km}{M} + 2\pi\frac{ln}{N}\right)\right]$$
$$+ i\frac{1}{MN}\sum_{k=0}^{M-1}\sum_{l=0}^{N-1}\left[R_{\chi_{kl}}\sin\left(2\pi\frac{km}{M} + 2\pi\frac{ln}{N}\right) + S_{\chi_{kl}}\cos\left(2\pi\frac{km}{M} + 2\pi\frac{ln}{N}\right)\right]$$

For real-valued X, the imaginary part for the uncertainty propagation can be neglected. Therefore, only the real part is considered.

$$X_{mn} = \frac{1}{MN}\sum_{k=0}^{M-1}\sum_{l=0}^{N-1}\left[R_{\chi_{kl}}\cos\left(2\pi\frac{km}{M} + 2\pi\frac{ln}{N}\right) - S_{\chi_{kl}}\sin\left(2\pi\frac{km}{M} + 2\pi\frac{ln}{N}\right)\right]$$

Sensitivity coefficients of input quantities χ_{kl}:

$$\frac{\partial X_{mn}}{\partial R_{\chi_{kl}}} = \frac{1}{MN}\cos\left(2\pi\frac{km}{M} + 2\pi\frac{ln}{N}\right)$$

$$\frac{\partial X_{mn}}{\partial S_{\chi_{kl}}} = \frac{1}{MN}\sin\left(2\pi\frac{km}{M} + 2\pi\frac{ln}{N}\right)$$

Uncertainty of X_{mn}:

$$\boldsymbol{R}(\boldsymbol{u}^2_{\boldsymbol{X_{mn}}}) \equiv \sum_{k=0}^{M-1}\sum_{l=0}^{N-1}\left(\frac{\partial X_{mn}}{\partial R\chi_{kl}}\right)^2 \boldsymbol{R}(\boldsymbol{u}^2_{\boldsymbol{\chi_{kl}}}) + \sum_{k=0}^{M-1}\sum_{l=0}^{N-1}\left(\frac{\partial X_{mn}}{\partial S\chi_{kl}}\right)^2 \boldsymbol{S}(\boldsymbol{u}^2_{\boldsymbol{\chi_{kl}}})$$

Uncertainties of $\boldsymbol{F}$ in the real domain:

$$\boldsymbol{u}^2_{\boldsymbol{F_{mn}}} = \frac{\boldsymbol{1}}{(\boldsymbol{MN})^2}\left[\sum_{\boldsymbol{m=0}}^{\boldsymbol{M-1}}\sum_{\boldsymbol{n=0}}^{\boldsymbol{N-1}}\boldsymbol{\cos^2}\left(\boldsymbol{2\pi}\frac{\boldsymbol{km}}{\boldsymbol{M}} + \boldsymbol{2\pi}\frac{\boldsymbol{ln}}{\boldsymbol{N}}\right)\boldsymbol{u}^2_{\boldsymbol{R_F}} + \sum_{\boldsymbol{m=0}}^{\boldsymbol{M-1}}\sum_{\boldsymbol{n=0}}^{\boldsymbol{N-1}}\boldsymbol{\sin^2}\left(\boldsymbol{2\pi}\frac{\boldsymbol{km}}{\boldsymbol{M}} + \boldsymbol{2\pi}\frac{\boldsymbol{ln}}{\boldsymbol{N}}\right)\boldsymbol{u}^2_{\boldsymbol{S_F}}\right]$$

4.3 Uncertainty propagation based on Wiener filter

Begin from the definition of the Wierner filter in the deconvolution process, each input function is rewritten with its real and imaginary parts:

$$R_F = \frac{R_G R_H + S_G S_H}{R_H^2 + S_H^2 + \alpha}$$

$$S_F = -\frac{R_G S_H - S_G R_H}{R_H^2 + S_H^2 + \alpha}$$

Sensitivity coefficients of input quantities R_G, S_G, R_H, S_G and α can be written as follows:

The real part:

$$R_{RG} = \frac{\partial R_F}{\partial R_G} = \frac{R_H}{R_H^2 + S_H^2 + \alpha}$$

$$R_{SG} = \frac{\partial R_F}{\partial S_G} = \frac{S_H}{R_H^2 + S_H^2 + \alpha}$$

$$R_{RH} = \frac{\partial R_F}{\partial R_H} = \frac{R_G(S_H^2 - R_H^2 + \alpha) - 2S_G R_H S_H}{(R_H^2 + S_H^2 + \alpha)^2}$$

$$R_{SH} = \frac{\partial R_F}{\partial S_H} = \frac{S_G(R_H^2 - S_H^2 + \alpha) - 2R_G R_H S_H}{(R_H^2 + S_H^2 + \alpha)^2}$$

$$R_\alpha = \frac{\partial R_F}{\partial \alpha} = -\frac{R_G R_H + S_G S_H}{(R_H^2 + S_H^2 + \alpha)^2}$$

The imaginary part:

$$S_{RG} = \frac{\partial S_F}{\partial R_G} = -\frac{S_H}{R_H^2 + S_H^2 + \alpha}$$

$$S_{SG} = \frac{\partial S_F}{\partial S_G} = \frac{R_H}{R_H^2 + S_H^2 + \alpha}$$

$$S_{RH} = \frac{\partial S_F}{\partial R_H} = \frac{S_G(S_H^2 - R_H^2 + \alpha) + 2R_G R_H S_H}{(R_H^2 + S_H^2 + \alpha)^2}$$

$$S_{SH} = \frac{\partial S_F}{\partial S_H} = -\frac{R_G(R_H^2 - S_H^2 + \alpha) + 2S_G R_H S_H}{(R_H^2 + S_H^2 + \alpha)^2}$$

$$S_\alpha = \frac{\partial S_F}{\partial \alpha} = -\frac{R_G S_H - S_G R_H}{(R_H^2 + S_H^2 + \alpha)^2}$$

Uncertainty of *F* in the Fourier domain:

The real part:

$$\boldsymbol{u_{R_F}^2 \equiv (R_{RG})^2 u_{RG}^2 + (R_{SG})^2 u_{SG}^2 + (R_{RH})^2 u_{RH}^2 + (R_{SH})^2 u_{SH}^2 + (R_\alpha)^2 u_\alpha^2}$$

The imaginary part:

$$\boldsymbol{u_{S_F}^2 \equiv (S_{RG})^2 u_{RG}^2 + (S_{SG})^2 u_{SG}^2 + (S_{RH})^2 u_{RH}^2 + (S_{SH})^2 u_{SH}^2 + (S_\alpha)^2 u_\alpha^2}$$

4.4 Uncertainty evaluation for the tip calibration

Uncertainty evaluation for the tip calibration process is based on the definition in the Section 3.3 of Appendix A.

4.4.1 Uncertainty in the real domain

Uncertainty of input quantities ***G***:

$$\boldsymbol{u_G^2 \equiv u_{\Delta\phi}^2}$$

4.4.2 Uncertainty for H in the Fourier domain

$$H(\boldsymbol{k}, z) \equiv -[LCF]^2 m(\boldsymbol{k}) \cdot (1 - e^{-kh}) \cdot e^{-kz} = (1 - e^{-kh}) \cdot e^{-kz} \cdot (R_\sigma + iS_\sigma)$$

$$R_H \equiv (1 - e^{-kh}) \cdot e^{-kz} \cdot R_\sigma$$

$$S_H \equiv (1 - e^{-kh}) \cdot e^{-kz} \cdot S_\sigma$$

$$\boldsymbol{u_{RH}^2 = k^2 R_H^2 u_z^2 + \left(k \cdot e^{-kh} \cdot e^{-kz}\right)^2 R_\sigma^2 \cdot u_h^2}$$

$$\boldsymbol{u_{SH}^2 = k^2 S_H^2 u_z^2 + \left(k \cdot e^{-kh} \cdot e^{-kz}\right)^2 S_\sigma^2 \cdot u_h^2}$$

4.4.3 Uncertainty of α in the Fourier domain

From Wiener deconvolution method, the uncertainty of $\log^\alpha$ is considered as $\mathbf{u_{log\alpha}}$, thus,

$$u_\alpha^2 = \left(\alpha \ln^{10} u_{log\alpha}\right)^2$$

4.4.4 Uncertainty of TTF in the real domain

The combined uncertainty of *TTF*, in the real domain with all contributions of the uncertainties of the input quantities i.e. Q, C_{tip}, M_S, δA_{pixel}, and u_F, can be written as:

$$u_{TTF\_B}^2 = \overline{TTF}^2 \left[\left(\frac{u_Q}{Q} \right)^2 + \left(\frac{u_{C_{tip}}}{C_{tip}} \right)^2 + \left(\frac{u_{M_S}}{M_S} \right)^2 + \left(\frac{u_{\delta A}}{\delta A} \right)^2 \right] + \frac{1}{C_0^2} u_F^2$$

4.4.5 Standard uncertainty of TTF

$$u_{TTF}^2 = u_{TTF\_A}^2 + u_{TTF\_B}^2$$

4.4.6 Expanded uncertainty

For a confidence level of 95%, a coverage factor k=2 is recommended.

$$U_{TTF} = k u_{TTF} = 2 u_{TTF}$$

4.5 Uncertainty evaluation for the stray field evaluation

Uncertainty evaluation for the tip calibration process is based on the definition in the Section 4 of Appendix A.

4.5.1 Uncertainty in the real domain

Uncertainty of input quantities ***G***:

$$u_G^2 \equiv u_{\Delta\phi}^2$$

4.5.2 Uncertainty for H in the Fourier domain

$$H(\boldsymbol{k}, z) \equiv -[LCF]^2 \widehat{H}_{TTF}(\boldsymbol{k}, z) = -[R_{LCF^2} + iS_{LCF^2}] \cdot [R_{TTF} - iS_{TTF}]$$

$$R_H = [R_{LCF^2} R_{TTF} + S_{LCF^2} S_{TTF}]$$

$$S_H = [S_{LCF^2} R_{TTF} - R_{LCF^2} S_{TTF}]$$

$$u_{RH}^2 = R_{LCF^2}^2 \cdot u_{R_{TTF}}^2 + S_{LCF^2}^2 \cdot u_{S_{TTF}}^2$$

$$u_{SH}^2 = S_{LCF^2}^2 \cdot u_{R_{TTF}}^2 + R_{LCF^2}^2 \cdot u_{S_{TTF}}^2$$

4.5.3 Uncertainty of α in the Fourier domain

From Wiener deconvolution method, the uncertainty of $\log^{\alpha}$ is considered as $\mathbf{u_{log\alpha}}$, thus,

$$u_\alpha^2 = \left(\alpha \ln^{10} u_{log\alpha} \right)^2$$

4.5.4 Uncertainty of stray field H_z^S in the real domain

The combined uncertainty of H_z^S in the real domain includes the uncertainty contributions resulting from Q, C_{tip}, δA_{pixel}, and u_F, can be written as:

$$u_{HZ\_B}^2 \equiv H_z^{S^2} \left[\left(\frac{u_Q}{Q} \right)^2 + \left(\frac{u_{C_{tip}}}{C_{tip}} \right)^2 + \left(\frac{u_{\delta A}}{\delta A} \right)^2 \right] + \frac{1}{C_1^2} u_F^2$$

4.5.5 Standard uncertainty of H_z^S

$$u_{HZ}^2 = u_{HZ\_A}^2 + u_{HZ\_B}^2$$

4.5.6 Expanded uncertainty

For a confidence level of 95%, a coverage factor k=2 is recommended.

$$U_{HZ} = k u_{HZ} = 2 u_{HZ}$$

5. Monte Carlo Technique

Alternatively, the uncertainty of TTF or H_z^S can be also calculated based on the Monte Carlo Technique [22]. For a single scan, input quantities are assumed to be a normal distribution formed by input quantity values and their standard deviation. Taking a "random value" from the distribution for each input quantity and perform tip calibration or stray field determination process. Repeat this procedure for N times (N > 1000). The target quantity and its standard uncertainty can be obtained:

$$\overline{\boldsymbol{Y}} = \frac{\boldsymbol{1}}{\boldsymbol{N}} \sum_{\boldsymbol{i=1}}^{\boldsymbol{N}} \boldsymbol{Y_i}$$

$$\boldsymbol{s_Y^2} = \frac{\boldsymbol{1}}{\boldsymbol{N-1}} \sum_{\boldsymbol{i=1}}^{\boldsymbol{N}} (\boldsymbol{Y_i} - \overline{\boldsymbol{Y}})^{\boldsymbol{2}}$$

References

[1] M. Seifert, V. Neu, and L. Schultz: "Epitaxial SmCo5 thin films with perpendicular anisotropy", Appl. Phys. Lett, vol. 94, 022501 (2009).

[2] H.J. Hug, B. Stiefel, P.J.A. van Schendel, A. Moser, R. Hofer, S. Martin, H.-J. Güntherodt, S. Porthun, L. Abelmann, J.C. Lodder, G. Bochi, and R.C. O'Handley: "Quantitative magnetic force microscopy on perpendicularly magnetized samples,"J. Appl. Phys. vol. 83, no.11, pp. 5609-5620, June 1998.

[3] P.J.A. van Schendel, H.J. Hug, B. Stiefel, S. Martin, and H.-J. Güntherodt: "A method for the calibration of magnetic force microscopy tips," J. Appl.Phys., vol. 88, no. 1, pp. 435-445, July 2000.

[4] E. Meyer, H.J. Hug, and R. Bennewitz: „Scanning Probe Microscopy", Berlin Heidelberg, Germany: Springer-Verlag, 2004, ch. 4, pp. 96-115.

[5] M.A. Marioni, M. Penedo, M. Baćani, J. Schwenk, and H.J. Hug: "Halbach effect at the nanoscale from chiral spin textures," Nano Lett., vol. 18, no. 4, pp. 2263-2267, March, 2018.

[6] D. Nečas, P. Klapetek, V. Neu, M. Havlíček, R. Puttock, O. Kazakova, X. Hu, and L. Zajíčková: "Determination of tip transfer function for quantitative MFM using frequency domain filtering and least squares method," Sci. Rep. vol. 9, p. 3880, March 2019.

[7] S. Vock, Z. Sasvári, C. Bran, F. Rhein, U. Wolff, N.S. Kiselev, A.N. Bogdanov, L. Schultz, O. Hellwig, and V. Neu: "Quantitative magnetic force microscopy study of the diameter evolution of bubble domains in a (Co/Pd)80 multilayer," IEEE Trans. Magn., vol. 47, no. 10, pp. 2352-2355, Oct. 2011.

[8] S. Vock, C. Hengst, M. Wolf, K. Tschulik, M. Uhlemann, Z. Sasvári, D. Makarov, O.G. Schmidt, L. Schultz, and V. Neu: "Magnetic vortex observation in FeCo nanowires by quantitative magnetic force microscopy," Appl. Phys. Lett., vol. 105, no. 17, p. 172409, Oct. 2014.

[9] N. Wiener: "Extrapolation, interpolation and smoothing of stationary time series, with engineering applications," Eastford, CT, USA, Martino Fine Books, 2013.

[10] P.C. Hansen: "The L-Curve and Its Use in the Numerical Treatment of Inverse Problems", in Computational Inverse Problems in Electrocardiology, ed. P. Johnston, Advances in Computational Bioengineering, PP. 119-142 (2000).

[11] O. Wolter, Th. Bayer, and J. Greschner: “Micromachined silicon sensors for scanning force microscopy,” J. Vac. Sci. Technol. B, vol. 9, no. 2, pp. 1353-1357, March 1991.

[12] S. Gao, U. Brand, S. Hahn, and K. Hiller: “An active reference spring array for in-situ calibration of the normal spring constant of AFM cantilevers,” in SPIE 9517 Smart sensors, Actuators and MEMS VII; and Cyber Physical Systems, p. 951719, 2015.

[13] D. Sarid: “Scanner force microscopy,” edited by M. Lapp and H. Stark, Oxford University Press, New York, 1991, p. 21.

[14] O. Kazakova, R. Puttock, C. Barton , H. Corte-León, M. Jaafar, V. Neu, and A. Asenjo: “Frontiers of magnetic force microscopy”, J. Appl. Phys., vol. 125, 060901 (2019).

[15] X.K. Hu, et al.: “Uncertainty propagation and evaluation of nano-scale stray field in quantitative magnetic force microscopy measurements,” presented at CPEM 2018, Paris, France, July 8-13, 2018.

[16] I. Horcas, R. Fernández, J. M. Gómez-Rodríguez, J. Colchero, J. Gómez-Herrero, and A. M. Baro: “SXM: A software for scanning probe microscopy and a tool for nanotechnology”, Rev. Sci. Instrum., Vol. 78, 013705 (2007).

[17] Nečas, D., Klapetek, P.: „Gwyddion: an open-source software for SPM data analysis“, Cent. Eur. J. Phys., 10, 181–188 (2012).

[18] S Eichstädt, V Wilkens: “GUM2DFT—a software tool for uncertainty evaluation of transient signals in the frequency domain”, Measurement Science and Technology, vol. 27, No. 5, 2016.

[19] EUROLAB Technical Report 1/2006, “Guide to the Evaluation of Measurement Uncertainty for Quantitative Test Results”, August 2006.

[20] Johannes Schwenk: “Multi-modal and quantitative Magnetic Force Microscopy- Application to Thin Film Systems with interfacial Dzyaloshinskii-Moriya Interaction”, 2016.

[21] M.D. DeJong, K.L. Livesey: “Analytic theory for the switch from Bloch to Néel domain wall in nanowires with perpendicular anisotropy”, Phys. Rev. B 92, 214420 (2015).

[22] M. Cox, M. Dainton, P. Harris: “Software specifications for Uncertainty Calculation”, NPL Report MSC 40/04 (2004).